Relevant out-of-time-order correlator operators: Footprints of the classical dynamics

Pablo D. Bergamasco

Departamento de Física, CNEA, Libertador 8250, C1429BNP Buenos Aires, Argentina

Gabriel G. Carlo and Alejandro M. F. Rivas

Departamento de Física, CNEA, CONICET, Libertador 8250, C1429BNP Buenos Aires, Argentina

The out-of-time-order correlator (OTOC) has recently become relevant in different areas where it has been linked to scrambling of quantum information and entanglement. It has also been proposed as a good indicator of quantum complexity. In this sense, the OTOC-RE theorem relates the OTOCs summed over a complete basis of operators to the second Renyi entropy. Here we have studied the OTOC-RE correspondence on physically meaningful bases like the ones constructed with the Pauli, reflection, and translation operators. The evolution is given by a paradigmatic bi-partite system consisting of two perturbed and coupled Arnold cat maps with different dynamics. We show that the sum over a small set of relevant operators is enough in order to obtain a very good approximation for the entropy and, hence, to reveal the character of the dynamics. In turn, this provides us with an alternative natural indicator of complexity, i.e., the scaling of the number of relevant operators with time. When represented in phase space, each one of these sets reveals the classical dynamical footprints with different depth according to the chosen basis.

I. INTRODUCTION

There is a great interest in the out-of-time-order correlator (OTOC) nowadays, coming from different areas like high energy and gravity, condensed matter, many-body systems, quantum information, and quantum chaos. This measure has been introduced in the superconductivity context [1] where its exponential growth as a function of time has been associated with chaotic behavior. The OTOC is usually defined as a four-point out-of-time order correlator,

$$C(t) = \langle \hat{M}(t)\hat{V}(0)\hat{M}(t)\hat{V}(0) \rangle, \quad (1)$$

where $\langle \cdot \rangle = \text{Tr}[\rho \cdot]/N$, with ρ being an arbitrary initial state. In many works $\langle \cdot \rangle = \text{Tr}[\cdot]/N$ is taken as the thermal average, an approach that we follow. Finally, $M(t)$ is an operator evolved in the Heisenberg picture. Establishing an upper limit to the growth rate of the OTOC in black hole models [2] has led to a surge in the interest in this versatile measure. Examples can be found in many-body physics [3–10], quantum chaos [11–13], high-energy physics [14], and the link between topological gravity and quantum chaos [15]. Recently, the OTOC behavior has been studied for bipartite systems. In Ref. [16] it was found that for the chaotic case the scrambling process has two phases, one in which the exponential growth is within the subsystem and a second one which only depends on the interaction. In Ref. [17] the OTOC has proven to be a very good indicator of quantum complexity [18,19] when considering all possible dynamical scenarios.

The OTOC is conceptually related to scrambling of quantum information [20–22] and entanglement [17]. It is in this respect that the OTOC–Renyi entropy (OTOC-RE) theorem

[23,24] establishes the equivalence of the linear entropy S_L with the four-point OTOC averaged over a complete operator basis of some arbitrary partition of the system. Following the scheme presented in Ref. [24], we can summarize the theorem as

$$S_L = 1 - \text{Tr}[\hat{\rho}_A^2] = 1 - \sum_{\hat{M} \in B} \text{Tr}[\hat{M}(t)\hat{\rho}(0)\hat{M}^\dagger(t)\hat{\rho}(0)], \quad (2)$$

where A and B are two partitions of the system, $\hat{\rho}(0)$ is the initial (nonevolving) density operator of the whole system ($\hat{\rho}_A$ is the partial trace over subsystem B of $\hat{\rho}$), and S_L is the linear entropy. In the original form of the theorem the expression $1 - e^{(-S_A^{(2)})}$ is used for S_L in order to make a direct connection with $S_A^{(2)} = -\log \text{Tr}[\hat{\rho}_A^2]$, which is the second Renyi entropy. The $\hat{M}$ operators act on the subsystem B and define a complete basis normalized according to $\sum_{\hat{M} \in B} M_{ij}(M_{lm})^\dagger = \delta_{im}\delta_{lj}$. In Eq. (2) we have taken the second evolved operator as $\hat{M}^\dagger(t)$, being the transpose and conjugate of the first one in such a way to extend the validity of the theorem to unitary operators. The sum running over a complete basis characterizes the behavior of the OTOC of a given operator that belongs to it; this is remarkable since it bridges the gap between an inherently dynamical concept like the OTOC and an information theoretical one like the entropy. This result prescribes an average behavior for different OTOCs in a given basis, but it is important to ask ourselves how meaningful this is. As a matter of fact, is each one of the terms appearing in Eq. (2) equally relevant, making the same contribution to the linear entropy? In this work we determine that not all of the OTOCs are good indicators of quantum complexity, but we are able to

classify them in terms of the information they provide about the dynamical features.

Our system consists of two perturbed and coupled Arnold cat maps with different dynamics. The three possible cases were considered, i.e., both maps being hyperbolic (chaotic) (HH), both elliptic (regular) (EE), and a mixed scenario where one map is hyperbolic and the other is elliptic (HE,EH) [17]. Our objective with these choices, including the ones we call mixed (we do not refer to mixed in the Kolmogorov Arnold Moser (KAM) sense) is just to find the dependence of the OTOC behavior on all possible dynamical scenarios for each partition of the system. Also, we have considered three different bases constructed with Pauli or SU(N) operators, translation operators, and reflection operators on the torus [25]. In all cases we have taken the nonevolving density operator as a localized pure state. Our results show that when we perform the summation in Eq. (2) with a set of only 35% or less of the operators, in any of the chosen basis, 80% of S_L is recovered. On the other hand, this set of relevant operators is given by those that best capture the dynamics of the system, being suitable for complexity measures. For reflection and translation bases, they show clear footprints of the underlying classical dynamics in phase space.

This paper is organized as follows. In Sec. II we present our system with a brief description of the properties of the Hilbert space on the torus. We also describe the operator bases that we use for the OTOC-RE theorem analysis. In Sec. III we explain our results in detail, and in Sec. IV we state our conclusions.

II. SYSTEM AND BASES

The periodicity of the torus implies Bloch boundary conditions for wave functions:

$$\Psi(q + 1) = e^{2\pi i \chi_p} \Psi(q),$$
$$\tilde{\Psi}(p + 1) = e^{2\pi i \chi_q} \tilde{\Psi}(p),$$

where

$$\tilde{\Psi}(p) = \frac{1}{\sqrt{2\pi\hbar}} \int e^{-ipq/\hbar} \Psi(q) dq,$$

with $2\pi i \chi_p$ and $2\pi i \chi_q$ being arbitrary Floquet angles that determine the so-called prequantization. The values of χ_p and χ_q can be chosen in the range [0,1], we take $\chi_p = \chi_q = 0$. The previous boundary conditions can be satisfied if there is an integer N, so that [26]

$$\hbar = \frac{1}{2\pi N}. \tag{3}$$

This implies a Hilbert space, $\mathcal{H}_N$, of finite dimension N. We take $|q_n\rangle$ and $|p_m\rangle$ with $n, m = 0, 1, \ldots, N - 1$ as bases of $\mathcal{H}_N$. The states $\langle q|q_j\rangle$ are periodic Dirac δ distributions at positions $q = n/N \mathrm{mod}(1)$, with n being an integer in $[0, N - 1]$. These bases have the following normalization conditions,

$$\langle q_m|q_n\rangle = \langle p_m|p_n\rangle = \delta_{m,n}^{(N)},$$

with $\delta_{i,j}^{(N)}$ being the N-periodic Kronecker δ defined as

$$\delta_{i,j}^{(N)} = \sum_{k=-\infty}^{\infty} \delta_{i, j+kN}.$$

The bases are exchanged with the transformation kernel:

$$\langle p_m|q_n\rangle = \frac{1}{\sqrt{N}} e^{\frac{2\pi i m n}{N}}.$$

Position and momenta are then points in a discrete lattice on the torus with separation $1/N$, i.e., the quantum phase space [27].

The quantization of the cat map [28], which is one of the most simple paradigmatic models of chaotic dynamics, has helped to elucidate many questions in the quantum chaos area [28–31]. Here we consider the behavior of two coupled and perturbed cat maps, a two degrees of freedom example, which can have different types of dynamics. For each degree of freedom, the map is defined on the 2-Torus as [28]

$$\begin{pmatrix} q_{t+1} \\ p_{t+1} \end{pmatrix} = M \begin{pmatrix} q_t \\ p_t + \epsilon(q_t) \end{pmatrix}, \tag{4}$$

with q and p taken as modulo 1, and the perturbation

$$\epsilon(q_t) = -\frac{K}{2\pi} \sin(2\pi q_t).$$

The matrix M defines the dynamics. For the chaotic case we have chosen the hyperbolic map

$$M_h = \begin{pmatrix} 2 & 1 \\ 3 & 2 \end{pmatrix}, \tag{5}$$

while for the regular behavior we have taken the elliptic map

$$M_e = \begin{pmatrix} 0 & 1 \\ -1 & 0 \end{pmatrix}. \tag{6}$$

The propagator in the position representation is given by the $N \times N$ unitary matrix

$$U_{jk} = A \exp\left[\frac{i\pi}{NM_{12}}\left(M_{11}j^2 - 2jk + M_{22}k^2\right) + F\right], \tag{7}$$

where

$$A = [1/(iNM_{12})]^{1/2}$$

and

$$F = [iKN/(2\pi)]\cos(2\pi j/N)$$

(M_{ij} stands for the elements of the classical cat map evolution matrix). We can extend it to two degrees of freedom defined in a four-dimensional phase space of coordinates (q^1, q^2, p^1, p^2) [19] as

$$\begin{pmatrix} q_{t+1}^1 \\ p_{t+1}^1 \end{pmatrix} = M_1 \begin{pmatrix} q_t^1 \\ p_t^1 + \epsilon(q_t^1) + \kappa(q_t^1, q_t^2) \end{pmatrix}$$

and

$$\begin{pmatrix} q_{t+1}^2 \\ p_{t+1}^2 \end{pmatrix} = M_2 \begin{pmatrix} q_t^2 \\ p_t^2 + \epsilon(q_t^2) + \kappa(q_t^1, q_t^2) \end{pmatrix},$$

where the coupling between both maps is given by $\kappa(q_t^1, q_t^2)$. Hence, the quantum evolution for this case is given by the tensor product of the one degree of freedom maps

$$U_{j_1 j_2, k_1 k_2}^{\mathrm{2D}} = U_{j_1 k_1} U_{j_2 k_2} C_{j_1 j_2},$$

with the coupling matrix

$$C_{j_1 j_2} = \exp\left\{\left(\frac{iNK_c}{2\pi}\right)\cos\left[\frac{2\pi}{N}(j_1 + j_2)\right]\right\},$$

where $j_1, j_2, k_1, k_2 \in \{0, \ldots, N-1\}$. We fix $K = 0.25$ and $K_c = 0.5$ (Anosov condition [29]), and $N = 2^6$ throughout this work. We would like to underline that our map is unitary by construction; it inherits the unitarity of the map on the plane [28], and the perturbation and the coupling are defined by periodic functions on the torus [29].

For the complete set of operators spanning one of the subsystems in Eq. (2) we have chosen three different sets. They are the so-called computational or Pauli basis, the translation basis, and the reflection basis [25]. The first one is relevant for multiqubit systems (canonical in quantum computation and information), while the translation and reflection ones define the chord and Wigner (or center) functions [32], respectively, allowing for a more direct comparison with classical counterparts where centers and chords are canonically conjugated variables.

Pauli basis. For qubit systems, the typical basis chosen is $\{\sigma_0, \sigma_1, \sigma_2, \sigma_3\}$, where $\sigma_0 = \mathbb{1}$ and the rest of the σ_i's are 2×2 Pauli matrices. For dimensions $N = 2^k$, we can extend this basis by taking the complete system as a direct product of k single qubits:

$$\left\{ \bigotimes_{t=1}^{k} \sigma_{j_t} \right\}. \tag{8}$$

Translation and reflection bases. Translation operators $\hat{T}_\xi$ on the torus are described by the chord translation $\xi = (\xi_p, \xi_q) = (r/N, s/N)$, with r and s being integer indices. This unitary translation operators are defined in Ref. [25] by their action on the Hilbert space $\mathcal{H}_N$, such that

$$\hat{T}_{\xi(r,s)} |q_n\rangle = e^{i\frac{2\pi}{N} r(n + \chi_q + \frac{s}{2})} |q_{n+s}\rangle, \tag{9}$$

which translates the position state in q_n by a chord ξ_q to the position state in $q_{n+s} = q_n + \xi_q$. Analogously, acting on momentum states,

$$\hat{T}_{\xi(r,s)} |p_m\rangle = e^{-i\frac{2\pi}{N} s(m + \chi_p + \frac{r}{2})} |p_{m+r}\rangle \tag{10}$$

translates the momentum state in p_m by a chord ξ_p to the momentum state in $p_{m+r} = p_m + \xi_p$.

A complete basis of N^2 independent translation operators is obtained for chords performing up to one loop on the torus, that is, for r and s belonging to the interval $[0, N-1]$. The matrix elements of the translation operators $\hat{T}_\xi$ in the position representation are given by

$$\langle q_i| \hat{T}_{\xi(r,s)} |q_j\rangle = e^{i\frac{2\pi}{N} r(\frac{i+j}{2} + \chi_q)} \delta_{j,i+s}^{(N)} e^{-i\frac{2\pi}{N}(\frac{r}{2} + \chi_p)(j-i-s)}. \tag{11}$$

For the case of reflection operators $\hat{R}_x$, they are described by their center point $x = (x_p, x_q) = (a/N, b/N)$ with half-integer indices a and b. The reflection operators are defined in Ref. [25] by their action on the Hilbert space $\mathcal{H}_N$,

$$\hat{R}_{x(a,b)} |q_n\rangle = e^{i\frac{2\pi}{N}(2b-n)(a + \chi_q)} |q_{2b-n}\rangle, \tag{12}$$

which reflects the position state q_n through x_q to the position state in $q_{2b-n} = 2x_q - q_n$. Also, for momentum states,

$$\hat{R}_{x(a,b)} |p_m\rangle = e^{i\frac{2\pi}{N}(2a-m)(b + \chi_p)} |p_{2a-m}\rangle, \tag{13}$$

the operator reflects the state in p_m through the center x_p to the momentum state in $p_{2a-m} = 2x_p - p_m$. A complete
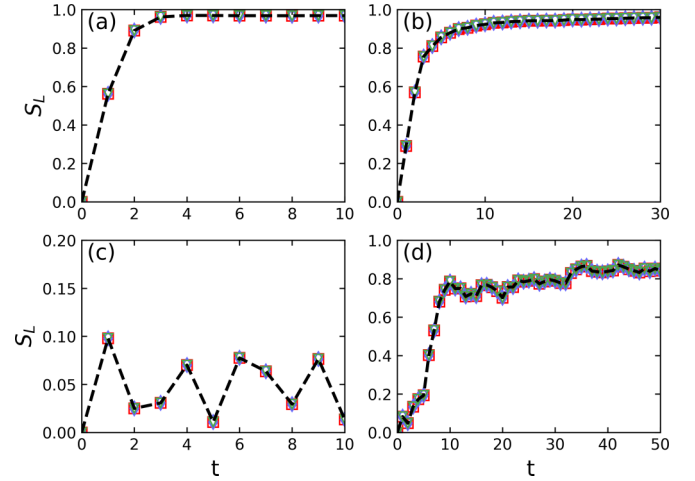

FIG. 1. In all panels we display S_L [(black) dashed line] [left-hand side of Eq. (2)] and the complete sum of OTOCs [right-hand side of Eq. (2)] for the three different bases described in the main text: Pauli or SU(N) [(red) squares], translations [(blue) diamonds], and reflections [(green) down triangles]. (a) HH case. (b) HE cases. (c) and (d) EE cases with the coherent states at $(q, p) = (0.5, 0.5)$ and $(q, p) = (\pi/4, \pi/4)$, respectively.

basis of N^2 independent reflection operators is obtained with half-integer indices a and b in $[0, \frac{N-1}{2}]$. That is, a quarter of the torus contains the complete information for the reflection basis [25].

The matrix elements in the position representation are

$$\langle q_i| \hat{R}_{x(a,b)} |q_j\rangle = e^{i\frac{2\pi}{N}(j-i)(a + \chi_q)} \delta_{j,2b-i}^{(N)} e^{i\frac{2\pi}{N} a(2b-i-j)}. \tag{14}$$

We recall that in both cases we have chosen the Floquet angles (χ_q, χ_p) as zero.

III. RESULTS

For completeness, we first check the validity of the OTOC-RE theorem [Eq. (2)] for all the dynamical scenarios and all the operator bases described in Sec. II. Figure 1(a) corresponds to S_L and all OTOCs sums as a function of the time t (map steps), for both dynamics being hyperbolic (HH), while in Figs. 1(b) and 1(c) we show the HE and EE cases, respectively. We consider a coherent state located at the fixed point $(q, p) = (0.5, 0.5)$ on each tori. Figure 1(d) displays the EE case where the coherent state is located at $(q, p) = (\pi/4, \pi/4)$ (not a fixed point). The theorem clearly holds regardless of the dynamics or the chosen basis.

We have classified each OTOC in Eq. (2) according to its contribution to the sum. In fact, their relevance is essentially given by the corresponding area under the curve up to a time t_0. We proceed in the following way: For each operator M we have calculated the area $A_M(t_0)$ as

$$A_M(t_0) = \int_0^{t_0} C_M(t) dt, \tag{15}$$

where $C_M(t)$ is the OTOC

$$C_M(t) = \text{Tr}[\hat{M}(t)\hat{\rho}(0)\hat{M}^\dagger(t)\hat{\rho}(0)]. \tag{16}$$
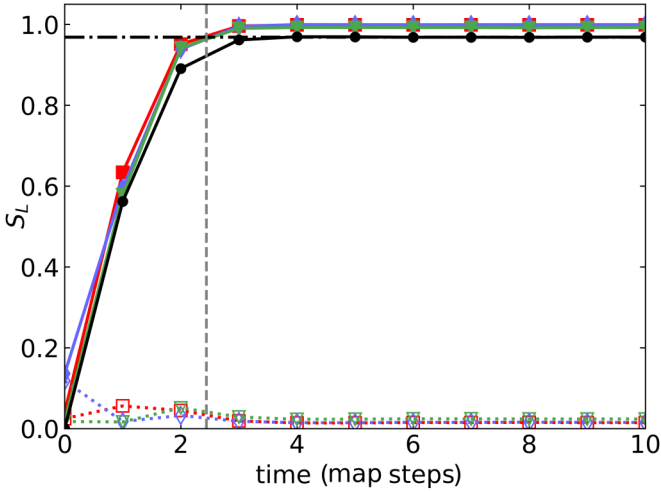
FIG. 2. S_L [(black) solid line with solid circles] given by the left-hand side of Eq. (2) for the HH case with coherent states taken at $(q, p) = (0.5, 0.5)$. Pauli [(red) solid line with solid squares] operators' sum considering the 263 most relevant terms in the right-hand side of Eq. (2). Translation [(blue) solid line with solid diamonds] and reflection [(green) solid line with solid down triangles] bases with 166 and 697 terms, respectively. Empty symbols with dotted lines show the contribution of the remaining terms for the Pauli [(red) dashed line with empty squares], translation [(blue) dashed line with empty diamonds], and reflection [(green) dashed line with empty down triangles] bases. $t_0 = 10$. We show the theoretical saturation value for the entropy by means of a dot-dashed horizontal line and the Ehrenfest time by means of a dashed vertical line.

FIG. 3. S_L [(black) solid line with solid circles] given by the left-hand side of Eq. (2) for the HE case with coherent states taken at $(q, p) = (0.5, 0.5)$. Pauli [(red) solid line with solid squares] operators' sum considering the 199 most relevant terms in the right-hand side of Eq. (2). Translation [(blue) solid line with solid diamonds] and reflection [(green) solid line with solid down triangles] bases with 110 and 1285 terms, respectively. Empty symbols with dotted lines show the contribution of the remaining terms for the Pauli [(red) dashed line with empty squares], translation [(blue) dashed line with empty diamonds], and reflection [(green) dashed line with empty down triangles] bases. $t_0 = 40$. We show the theoretical saturation value for the entropy by means of a dot-dashed horizontal line and the Ehrenfest time by means of a dashed vertical line.

Then, we have ordered the operators using $A_M(t_0)$, which reflects their contribution to the total area under $1 - S_L(t)$, given by $A_S(t_0) = \int_0^{t_0} 1 - S_L(t) dt$. Finally, we determine a cutoff criterion which consists of reaching the value $0.8 A_S(t_0)$ by simply adding the areas contributed by each operator's OTOC like $\sum_R A_M(t_0)$, where R means that the sum only runs from the most up to the least relevant one. This provides us with the number of OTOCs necessary to reach what we refer to as the effective S_L behavior.

We first consider the HH case with coherent states at $(q, p) = (0.5, 0.5)$. Due to the chaotic nature of the dynamics, both the OTOCs and S_L grow exponentially [17] at an early stage, hence we only look up to $t_0 = 10$. In Fig. 2 we show $S_L(t_0)$ (black lines) and the partial sum obtained with the most relevant OTOCs (solid symbols) for each operator basis. For the Pauli basis, only 263 from a total of 4096 terms were needed in order to reach the effective S_L behavior. Meanwhile, for the translation and reflection bases 166 and 697 terms were needed, respectively. The effective entropy behavior is recovered with less than 20% of the operators. In addition, in Fig. 2 we also show the contribution of the remaining OTOCs (empty symbols), which is markedly lower than that of the most relevant ones. We notice that in all figures we display $1 - \sum_R C_M(t)$, which is directly compared to S_L, and then the values corresponding to the empty symbols are subtracted from the solid ones to recover the entropy. Finally, it is important to mention that the saturation value of the entropy has been theoretically predicted with random matrix theory (see Ref. [18] and references therein); we display it by means
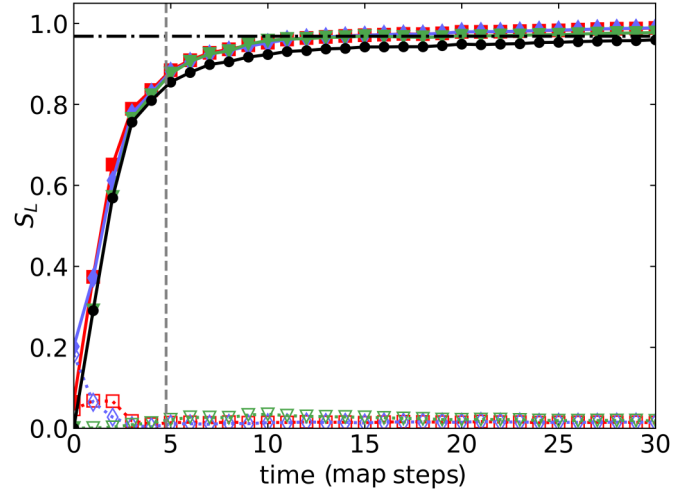
of a horizontal dot-dashed line. Also, we can observe that this saturation is reached at approximately the Ehrenfest time, which is shown by a vertical dashed line.

Next we look into the HE map where the operator basis is taken for the regular subsystem and coherent states are placed at $(q, p) = (0.5, 0.5)$. In Fig. 3 we see that S_L grows slower than in the previous case (until saturation) due to the mixed character of the dynamics, leading us to a longer integration time ($t_0 = 40$). To recover the effective S_L behavior this time, we needed 199 Pauli operators, 110 translation operators, and 1285 reflection operators, i.e., less than 32% of the total operators in the worst case. We also show the saturation value of the entropy and the Ehrenfest time, but in this case the agreement is not as good as in the previous case.

Finally, we take the EE map with coherent states at $(q, p) = (0.5, 0.5)$ and then at $(q, p) = (\pi/4, \pi/4)$. The first case is shown in Fig. 4 ($t_0 = 10$), where the effective S_L behavior is recovered by just 81 operators in the Pauli basis, 101 operators in the translation basis, and 117 operators in the reflection basis. In this dynamical scenario the coherent state does not explore the entire phase space but just rotates around the fixed point, giving a hint to explain this clear reduction in the number of relevant operators. In this case we have rescaled the partial sum of the most relevant OTOCs for a better comparison with S_L (the sum of the remaining ones is left unchanged). In Fig. 5 we display the results when placing the coherent states at $(q, p) = (\pi/4, \pi/4)$. Since this is not at a fixed point the entropy grows up to saturation at a slower rate than in the HH case, leading us to consider $t_0 = 30$.
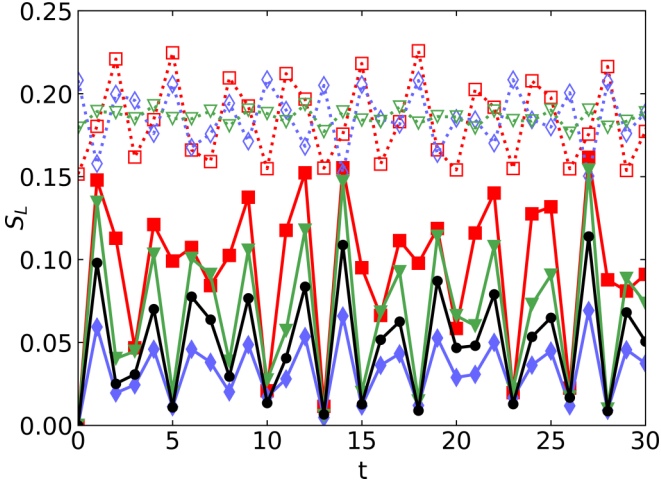
FIG. 4. S_L [(black) solid line with solid circles] given by the left-hand side of Eq. (2) for the EE case with coherent states taken at $(q, p) = (0.5, 0.5)$. Pauli [(red) solid line with solid squares] operators' sum considering the 81 most relevant terms in the right-hand side of Eq. (2). Translation [(blue) solid line with solid diamonds] and reflection [(green) solid line with solid down triangles] bases with 101 and 117 terms, respectively. Empty symbols with dotted lines show the contribution of the remaining terms for the Pauli [(red) dashed line with empty squares], translation [(blue) dashed line with empty diamonds], and reflection [(green) dashed line with empty down triangles] bases. $t_0 = 10$.
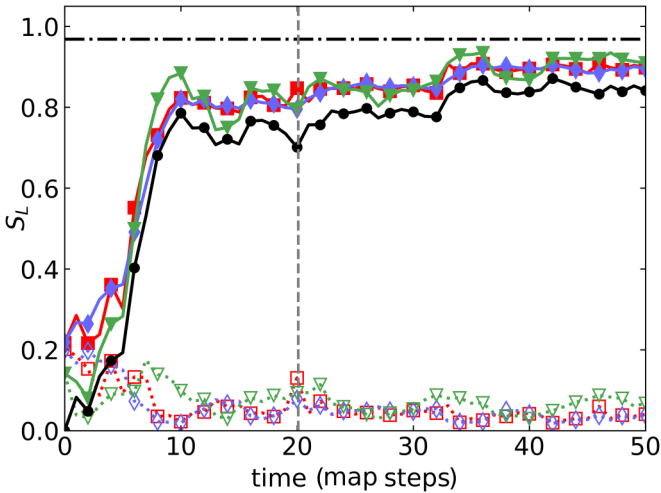

FIG. 5. S_L [(black) solid line with solid circles] given by the left-hand side of Eq. (2) for the EE case with coherent states taken at $(q, p) = (\pi/4, \pi/4)$. Pauli [(red) solid line with solid squares] operators' sum considering the 413 most relevant terms in the right-hand side of Eq. (2). Translation [(blue) solid line with solid diamonds] and reflection [(green) solid line with solid down triangles] bases with 103 and 1450 terms, respectively. Empty symbols with dotted lines show the contribution of the remaining terms for the Pauli [(red) dashed line with empty squares], translation [(blue) dashed line with empty diamonds], and reflection [(green) dashed line with empty down triangles] bases. $t_0 = 30$. We show the theoretical saturation value for the entropy by means of a dot-dashed horizontal line and the Ehrenfest time by means of a dashed vertical line.
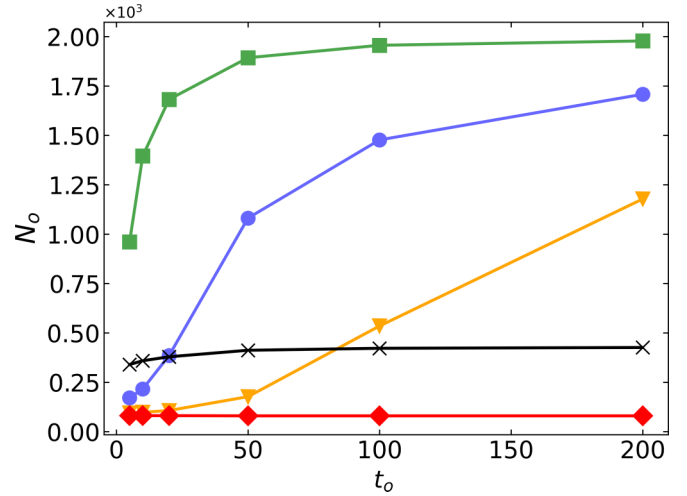

FIG. 6. Number of relevant Pauli operators, for different integration times t_0 and dynamics. The blue line with circles stands for the HH case, the green line with squares stands for the EH case, the orange line with down triangles stand for the HE case, and finally, the red line with diamonds and the black line with crosses stand for the EE cases with coherent states at $(0.5, 0.5)$ and $(\pi/4, \pi/4)$, respectively. $N = 2^6$.

We recover the effective S_L behavior with 413 operators in the Pauli basis, 103 in the translation basis, and 1450 in the reflection basis, i.e., about 35% of the operators in the worst case. The saturation and Ehrenfest time values are displayed in order to show the much slower convergence rate when compared to the HH case. We mention that not only the sum but also each one of the quantities $1 - C_{M_R}(t)$ (where $\hat{M}_R$ stands for the relevant operators) approximates the linear entropy very well (up to normalization); i.e., we claim that $S_L = 1 - e^{(-S_A^{(2)})} \approx 1 - C_{M_R}(t)$. The remaining operators have a different behavior.

On the other hand, it is interesting to investigate if the amount of relevant operators changes as a function of the integration time t_0 and eventually how this change is. In Figures 6, 7, and 8 we show the number of relevant operators for Pauli, translation, and reflection bases, respectively, for each dynamics and different integration times needed to achieve the effective S_L behavior. For all bases we notice that if the system has at least one hyperbolic degree of freedom, the number of operators grows steeply with the integration time. If the system is completely elliptic and the coherent states are located at the fixed point, the number of operators is essentially constant, while if they are not at a periodic orbit, the number of operators grows with a rate much slower than that in the mixed (HE and EH; we have taken both points of view in order to better look into dynamical properties) or totally hyperbolic (HH) cases, specially for the reflection basis (see Fig. 8). For the HH case, if we take long integration times, we will have that almost all operators (not all since we only require the effective S_L behavior) are relevant and equivalent, reminding us of the underlying classical ergodicity in this scenario. Growth in the number of relevant operators gives us more hints on the OTOCs sensitivity for quantum complexity, providing an alternative natural indicator of it.
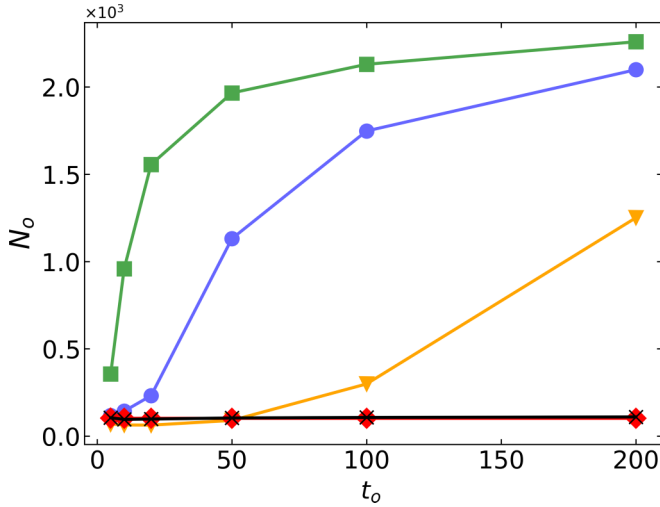
FIG. 7. Number of relevant translation operators, for different integration times t_0 and dynamics. Same color code as in Fig. 6. $N = 2^6$.

As a final remark, from Figs. 6, 7, and 8, we see that the number of relevant operators can be dependent on the basis. An extreme example is given by the Kirkwood one whose operators are defined by

$$K_{(i,j)} = |q_i\rangle \langle p_j| \tag{17}$$

and for which there is a clear association with phase space representations, having a direct classical meaning [11]. For any of the operators in this basis, it is straightforward to show that

$$C_{K(i,j)}(t) = \rho_A^2(t); \tag{18}$$

hence, all of them are equally relevant in sensing the dynamics, so special care must be taken at the time of selecting the basis if one wants to profit from the OTOCs ability to characterize quantum complexity.
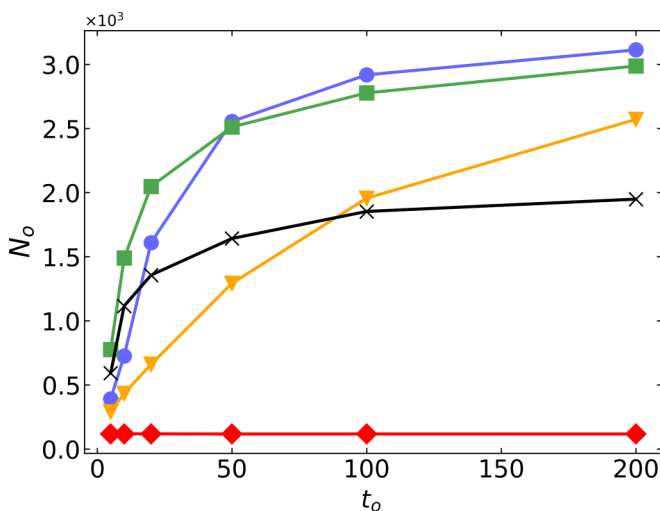

FIG. 8. Number of relevant reflection operators, for different integration times t_0 and dynamics. Same color code as in Fig. 6. In this case we have used $N = 2^6 + 1$ as the dimension of Hilbert space.
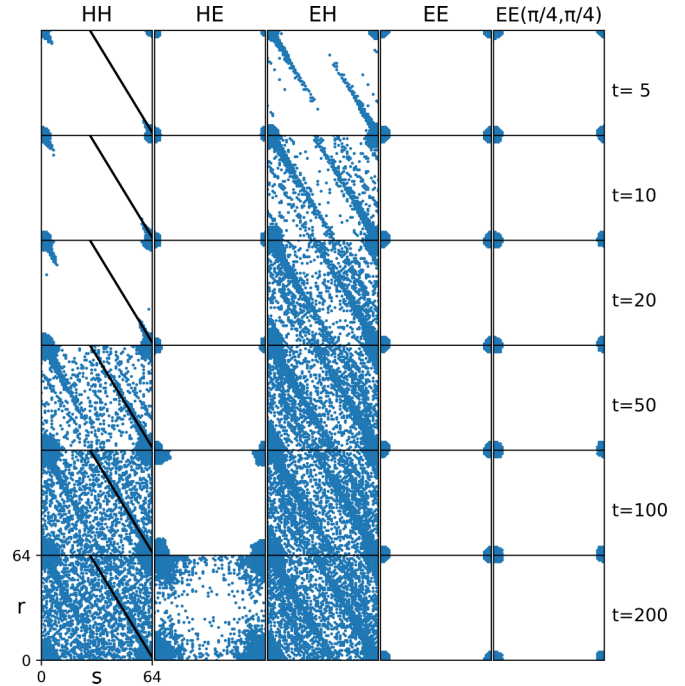

FIG. 9. Relevant translation operators in phase space, for each dynamics as we increase the integration time t_0. Each point (r, s) represents a translation chord, where r indicates the translation in momentum and s indicates the translation in position. The black solid line represents the unstable manifold direction of our map. $N = 2^6$.

All the previous analysis has led us to look for an explanation of the physical meaning of the operator relevance at the time to describe the S_L behavior or the quantum complexity in general. In order to proceed, we restrict ourselves to translation and reflection operators since they can be represented in chord and center phase space. In Eqs. (11) and (14), we identified each one of these operators with a couple of indexes, (r, s) for translations and (a, b) for reflections, which are related to the chord of translation and the reflection center, respectively. These indices can be represented in a two-dimensional plot, allowing one to visualize the different operators. Figures 9 and 10 show the most relevant translation and reflection operators for each dynamics and different integration times t_0. For reflections, we have chosen an odd Hilbert space dimension of $N = 65$ in order to deploy [25] the complete basis from the quarter torus with half-integer indices into the full one with integer indices. This allows a clearer visualization of the classical structures in phase space [33].

In the HH case, we see that the relevance of translation and reflection operators grows along the unstable manifold of our map, indicated in Figs. 9 and 10 with a black solid line. The number of relevant operators grows with t_0 and finally extends to the entire phase space. In the HE scenario, the relevant translation operators (see Fig. 9) are grouped around the identity operator (the chord is null) because we are looking at the elliptic degree of freedom. However, the number of them increases with t_0, reflecting the spreading of the coherent state due to the influence of the hyperbolic map. Relevant reflections are concentrated in the center of the phase space where the coherent state is (see Fig. 10), and when t_0 increases, more
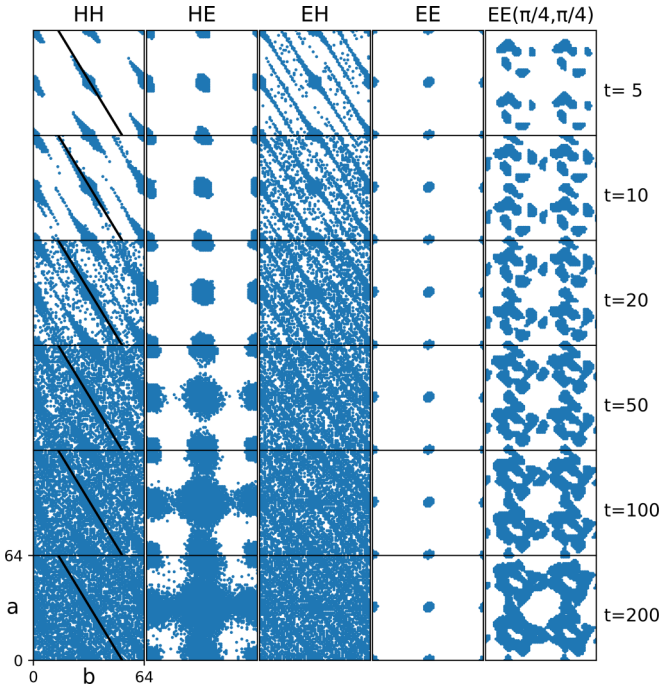
FIG. 10. Relevant reflection operators in phase space, for each dynamics as we increase the integration time t_0. Each point (a, b) represents a reflection center, where a indicates its momentum and b its position. The black solid line represents the unstable manifold direction of our map. In this case we have used $N = 2^6 + 1$ as the dimension of Hilbert space.

operators are needed to describe the dynamics enlarging the corresponding distribution. A similar situation arises in the EH case (now we observe the hyperbolic subsystem); i.e., the number of relevant operators grows and its distribution spreads along the unstable direction for both translations and reflections. Finally, in the EE case for the coherent state at the periodic point, the distributions remain localized and again the translation operators which better capture the dynamics are the ones closer to the identity, while the corresponding reflection operators are those at the center of the phase space. In both cases the number of relevant operators does not change. Finally, if we locate the coherent states out of the fixed point, the relevant translation operators are still closer to the identity, but the reflection ones follow the evolution of the distributions as in Ref. [18].

In all these cases, we can observe that the set of relevant operators follows the footprints of the classical dynamical evolution, and this provides us with a clear interpretation of the relevance criterion developed in this work. However, we underline that some bases of operators are more sensitive than others, following the footprints closer and allowing to the classical structures and the quantum complexity to be revealed in a clearer way. As we have previously seen in Eq. (18), for the Kirkwood basis all of the OTOCs are equivalent in

following the linear entropy behavior. For a pure state $\hat{\rho}$ with the translation operator basis, we can see that the OTOC can be expressed in terms of

$$\rho_\xi(t) = \mathrm{Tr}(\hat{T}_\xi \hat{\rho}(t)),$$

the chord representation of the evolved density $\hat{\rho}(t)$, as

$$C_{T\xi(t)} = \rho_\xi(t)\rho_{-\xi}(t). \tag{19}$$

Meanwhile, for the reflection basis, the OTOC can be expressed in terms of the Wigner function

$$W_x(t) = (2\pi\hbar)\mathrm{Tr}(\hat{R}_x\hat{\rho}(t))$$

as

$$C_{Rx(t)} = \frac{1}{(2\pi\hbar)^2}W_x^2(t). \tag{20}$$

This makes the OTOC in the reflection basis remarkably sensitive to the classical structures in phase space, providing a very clear link to complexity measures [19].

IV. CONCLUSIONS

Recently quantum chaos and high-energy physics have become closely related through a chaoticity measure, the OTOC. An interesting bridge towards a more general interpretation as a complexity measure has been provided from the quantum information perspective via the OTOC-RE theorem which relates it to the second Renyi entropy [17,23,24]. In this work we have deepened the study of this relation for a paradigmatic bipartite system covering the main kinds of dynamics, i.e., two coupled and perturbed Arnold cat maps. We have studied the behavior of three different bases of operators, namely the Pauli, translation, and reflection ones.

We have defined a criterion of relevance for each operator from these bases relying on their corresponding OTOC contribution to the linear entropy S_L up to time t_0. Armed with this tool we have found that less than 35% of the operators of these widely used bases is enough to reach the effective S_L behavior. This means that to characterize the system in terms of its complexity the whole basis of operators is not needed in general, but a much lower fraction is needed instead (we underline that this is basis dependent though). The least relevant operators have been revealed as poor indicators of the dynamical complexity of the system. Moreover, the scaling of the number of relevant operators as a function of the time t_0 proved to be an alternative indicator of complexity, much in the same sense as the scaling of the number of operations is a measure for algorithmic complexity.

Finally, for the translation and reflection operators which can be directly represented in phase space, our concept of relevance turns out to have an easy interpretation. The set of relevant operators follows the quantum footprints of the corresponding classical evolution (more or less closely depending on the basis). In the future we will investigate this relation even more deeply, taking into account generic density operators.

[1] A. I. Larkin and Yu. N. Ovchinnikov, Sov. Phys. JETP **28**, 1200 (1969).

[2] J. Maldacena, S. H. Shenker, and D. Stanford, J. High Energy Phys. **08** (2016)106.

[3] S. H. Shenker and D. Stanford, J. High Energy Phys. **03** (2014)067.

[4] I. L. Aleiner, L. Faoro, and L. B. Ioffe, Ann. Phys. (Amsterdam, Neth.) **375**, 378 (2016).

[5] Y, Huang, Y.-L. Zhang, and X. Chen, Ann. Phys. (Berlin) **529**, 1600318 (2017).

[6] F. Borgonovi and F. M. Izrailev, Phys. Rev. E **99**, 012115 (2019).

[7] K. Slagle, Z. Bi, Y. Z. You, and C. Xu, Phys. Rev. B **95**, 165136 (2017).

[8] X. Chen, T. Zhou, D. A. Huse, and E. Fradkin, Ann. Phys. (Berlin) **529**, 1600332 (2017).

[9] Q. Hummel, B. Geiger, J. D. Urbina, and K. Richter, Phys. Rev. Lett. **123**, 160401 (2019).

[10] E. M. Fortes, I. García-Mata, R. A. Jalabert, and D. A. Wisniacki, Europhys. Lett. **130**, 60001 (2020).

[11] A. Lakshminarayan, Phys. Rev. E **99**, 012201 (2019).

[12] I. García-Mata, M. Saraceno, R. A. Jalabert, A. J. Roncaglia, and D. A. Wisniacki, Phys. Rev. Lett. **121**, 210601 (2018).

[13] R. A. Jalabert, I. García-Mata, and D. A. Wisniacki, Phys. Rev. E **98**, 062218 (2018).

[14] T. Akutagawa, K. Hashimoto, T. Sasaki, and R. Watanabe, J. High Energ. Phys. **2020**, 13 (2020).

[15] Y. Liu and A. Raju, arXiv:2005.08508.

[16] R. Prakash and A. Lakshminarayan, Phys. Rev. B **101**, 121108(R) (2020).

[17] P. D. Bergamasco, G. G. Carlo, and A. M. F. Rivas, Phys. Rev. Res. **1**, 033044 (2019).

[18] P. D. Bergamasco, G. G. Carlo, and A. M. F. Rivas, Phys. Rev. E **96**, 062144 (2017).

[19] G. Benenti, G. G. Carlo, and T. Prosen, Phys. Rev. E **85**, 051129 (2012).

[20] S. Pappalardi, A. Russomanno, B. Žunkovič, F. Iemini, A. Silva, and R. Fazio, Phys. Rev. B **98**, 134303 (2018).

[21] M. Campisi and J. Goold, Phys. Rev. E **95**, 062127 (2017).

[22] B. Swingle, Nat. Phys. **14**, 988 (2018).

[23] P. Hosur, X. L. Qi, D. A. Roberts, and B. Yoshida, J. High Energy Phys. **02** (2016)004.

[24] R. Fan, P. Zhang, H. Shen, and H. Zhai, Sci. Bull. **62**, 707 (2017).

[25] A. M. F. Rivas and A. M. Ozorio de Almeida, Ann. Phys. **276**, 223 (1999).

[26] A. Bouzouina and S. De Bièvre, Commun. Math. Phys. **178**, 83 (1996).

[27] D. Galetti and A. F. R. De Toledo Piza, Phys. A (Amsterdam, Neth.) **149**, 267 (1988).

[28] J. H. Hannay and M. V. Berry, Phys. D (Amsterdam, Neth.) **1**, 267 (1980).

[29] M. Basilio De Matos and A. M. Ozorio De Almeida, Ann. Phys. **237**, 46 (1995).

[30] F. Haake, *Quantum Signatures of Chaos* (Springer-Verlag, New York, 2001).

[31] M. Degli Esposti and B. Winn, J. Phys. A: Math. Gen. **38**, 5895 (2005).

[32] A. M. Ozorio de Almeida, Phys. Rep. **295**, 265 (1998).

[33] A. M. F. Rivas, J. Phys. A: Math. Theor. **40**, 11057 (2007).